



OPEN ACCESS

EDITED BY

Diego Iacono,
Neuroscience - Uniformed Services University
of the Health Sciences (USU), United States

REVIEWED BY

Tohru Okanishi,
Tottori University, Japan
Ning Mao,
Yantai Yuhuangding Hospital, China

*CORRESPONDENCE

Yanwei Miao
✉ ywmiao716@163.com

[†]These authors have contributed equally to this work

SPECIALTY SECTION

This article was submitted to
Pediatric Neurology,
a section of the journal
Frontiers in Neurology

RECEIVED 30 May 2022

ACCEPTED 27 January 2023

PUBLISHED 14 February 2023

CITATION

Yu J, Liu Y, Jiang Y, Gao B, Wang J, Guo Y, Xie L
and Miao Y (2023) Development and evaluation
clinical-radiomics analysis based on
T1-weighted imaging for diagnosing neonatal
acute bilirubin encephalopathy.
Front. Neurol. 14:956975.
doi: 10.3389/fneur.2023.956975

COPYRIGHT

© 2023 Yu, Liu, Jiang, Gao, Wang, Guo, Xie and
Miao. This is an open-access article distributed
under the terms of the [Creative Commons
Attribution License \(CC BY\)](#). The use,
distribution or reproduction in other forums is
permitted, provided the original author(s) and
the copyright owner(s) are credited and that
the original publication in this journal is cited, in
accordance with accepted academic practice.
No use, distribution or reproduction is
permitted which does not comply with these
terms.

Development and evaluation clinical-radiomics analysis based on T1-weighted imaging for diagnosing neonatal acute bilirubin encephalopathy

Jinhong Yu^{1,2†}, Yangyingqiu Liu^{1†}, Yuhan Jiang¹, Bingbing Gao¹,
Jingshi Wang², Yan Guo³, Lizhi Xie⁴ and Yanwei Miao^{1*}

¹Department of Radiology, First Affiliated Hospital of Dalian Medical University, Dalian, Liaoning, China,

²Department of Radiology, Dalian Woman and Children's Medical Center (Group), Dalian, Liaoning, China,

³GE Healthcare, Life Science China, Shenyang, Liaoning, China, ⁴MRI Research, GE Healthcare, Beijing, China

Purpose: To investigate the value of clinical-radiomics analysis based on T1-weighted imaging (T1WI) for predicting acute bilirubin encephalopathy (ABE) in neonates.

Methods: In this retrospective study, sixty-one neonates with clinically confirmed ABE and 50 healthy control neonates were recruited between October 2014 and March 2019. Two radiologists' visual diagnoses for all subjects were independently based on T1WI. Eleven clinical and 216 radiomics features were obtained and analyzed. Seventy percent of samples were randomly selected as the training group and were used to establish a clinical-radiomics model to predict ABE; the remaining samples were used to validate the performance of the models. The discrimination performance was assessed by receiver operating characteristic (ROC) curve analysis.

Results: Seventy-eight neonates were selected for training (median age, 9 days; interquartile range, 7–20 days; 49 males) and 33 neonates for validation (median age, 10 days; interquartile range, 6–13 days; 24 males). Two clinical features and ten radiomics features were finally selected to construct the clinical-radiomics model. In the training group, the area under the ROC curve (AUC) was 0.90 (sensitivity: 0.814; specificity: 0.914); in the validation group, the AUC was 0.93 (sensitivity: 0.944; specificity: 0.800). The AUCs of two radiologists' and the radiologists' final visual diagnosis results based on T1WI were 0.57, 0.63, and 0.66, respectively. The discriminative performance of the clinical-radiomics model in the training and validation groups was increased compared to the radiologists' visual diagnosis ($P < 0.001$).

Conclusions: A combined clinical-radiomics model based on T1WI has the potential to predict ABE. The application of the nomogram could potentially provide a visualized and precise clinical support tool.

KEYWORDS

radiomics, acute bilirubin encephalopathy, magnetic resonance imaging, nomogram, hyperbilirubinemia

Introduction

Neonatal hyperbilirubinemia, characterized by jaundice, is a common and benign disease in neonates, but is the main cause of hospitalization in the first week after birth (1); neonatal jaundice is the seventh and the ninth cause of neonatal death in the early neonatal period (0–6 d) and late neonatal period (7–27 d), respectively (2, 3). Even though most hyperbilirubinemia

patients have a favorable prognosis, some severe cases may cause neurotoxicity and lead to neonatal acute bilirubin encephalopathy (ABE) (4) with a risk of neonatal mortality and life-long neurodevelopmental handicaps (5, 6).

Hyperintensity of the bilateral globus pallidus (GP) on T1-weighted imaging (T1WI) is considered to be a characteristic imaging manifestation of ABE (7, 8). However, the presence of myelin in these structures has also revealed hyperintensity on T1WI, which is easily confused with the changes caused by brain damage in ABE (9). Furthermore, hyperintensity on T1WI of GPs in neonates with ABE may be transient and subtle (7); the lack of objectivity and accuracy necessitates the need to determine GP signals by a radiologist's naked eye only, which may affect the early diagnosis and treatment of ABE, especially for those neonates who may have had early brain damage while the signal of GPs on T1WI has not increased. Therefore, conventional T1WI is insufficient to meet diagnostic needs. Radiomics is an emerging field that translates medical images into quantitative data (10, 11). The internal texture information of the GPs can be mined deeply by extracting high-throughput features, and the biological information can be displayed objectively and quantitatively.

The purpose of this study was to assess the value of a clinical-radiomics model based on T1WI for predicting ABE in neonates and to compare its diagnostic value with experienced radiologists' visual diagnosis results, providing a new tool for the early diagnosis and individualized monitoring of ABE.

Materials and methods

Patients

This retrospective study was approved by the hospital ethics committee and the requirement for informed consent was waived because of the retrospective nature of the study. One hundred and eleven neonates were recruited between October 2014 and March 2019. Figure 1 shows the pathway of ABE and healthy neonate inclusion and exclusion. Clinical features including age, gender, weight, gestational week, pregnancy history of maternal, meconium-stained amniotic fluid, premature rupture of membranes, singleton or multiple-birth pregnancy, and type of delivery were collected from all subjects. In order to construct a stable and generalization model, all subjects ($n = 111$) were randomly divided into a training group ($n = 78$) and a validation group ($n = 33$) according to the ratio of 7:3. The training group was used to construct models that were verified by the validation group.

MRI acquisition

All subjects underwent MRI examination on a GE Signa HDxT 1.5T MRI scanner with a dedicated eight-channel head and neck unite coil. Ten percent chloral hydrate (0.5 mL/kg) was administered *via* anal enema for sedation 30 min before examination. MRI

Abbreviations: T1WI, T1-weighted imaging; ABE, Acute bilirubin encephalopathy; ROC, Receiver operating characteristic; AUC, Area under the ROC curve; GP, Globus pallidus.

scanning was performed during the deep sedation. The imaging protocol included axial T1WI (TR = 2950 ms, TE = 25 ms, slice thickness = 4 mm, matrix = 288 × 192, NEX = 2, FOV = 22.0 × 22.0 cm).

Radiologists' visual diagnosis

Radiologist 1 (JY) and radiologist 2 (JW), with 15 and 20 years of experience in neonatal radiology, respectively, independently provided what they thought was the most likely diagnosis for all subjects ($n = 111$) based on T1WI. For the subjects with controversial diagnoses from radiologists 1 and 2, a review was conducted by radiologist 3 with 25 years of experience (YM) to determine the radiologists' final visual diagnosis. Radiologists were blinded to all clinical and diagnosis information except age at the time of MRI scanning. Images were displayed in a random sequence.

Segmentation and feature extraction

MRI data were transferred to a personal computer and processed based on 3D slicer software (<http://www.slicer.org>). The regions of interest were manually outlined along the boundary of the bilateral GPs on the slices with the largest area of bilateral GPs and its adjacent upper and lower slices on T1WI. Then, a volume of interest was automatically generated on the software. One hundred and six features of each GP (212 features of bilateral GPs) for each neonate were extracted by 3D slicer software. All radiomics features are summarized in [Supplementary material E1](#).

Feature selection and prediction model building

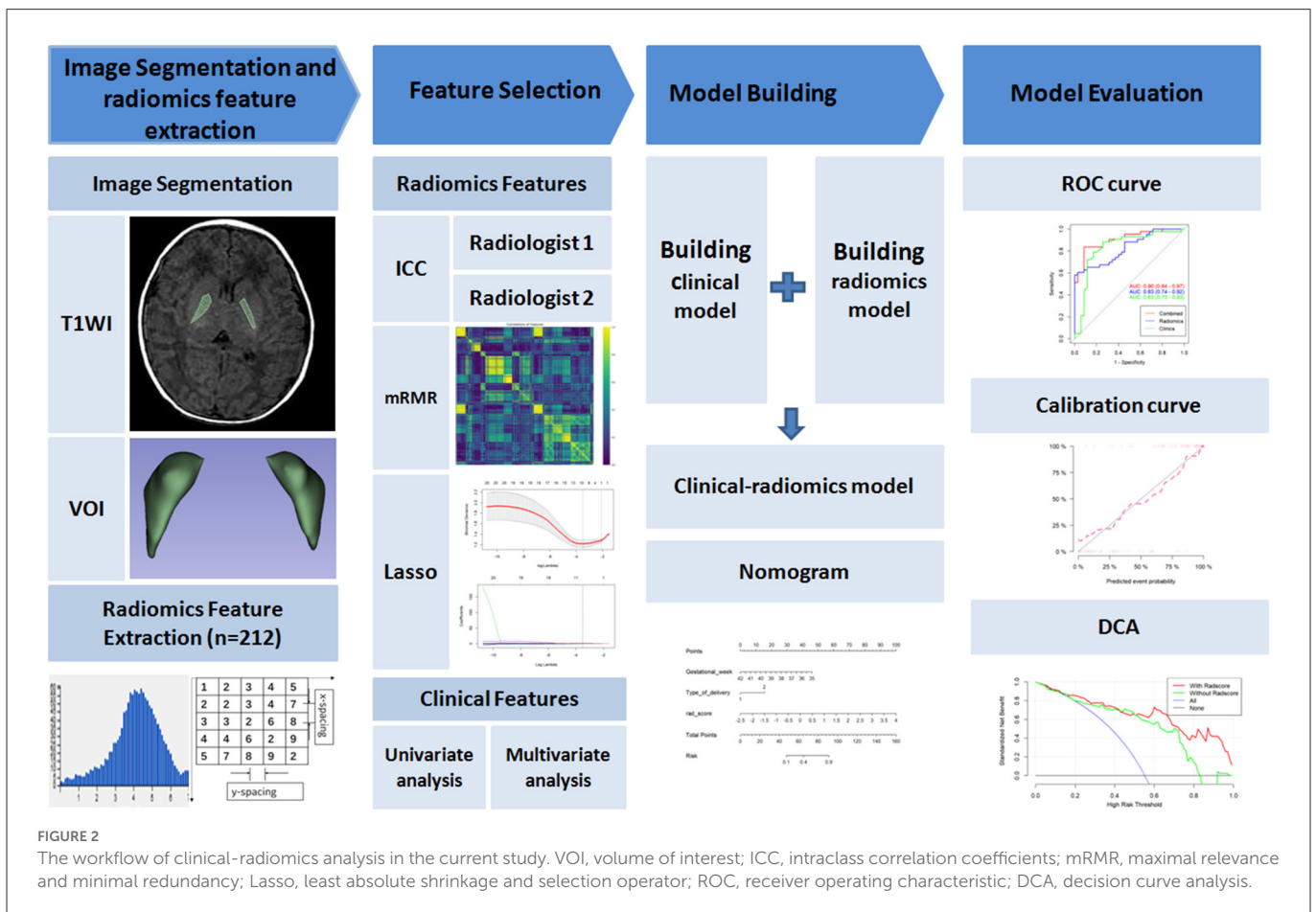
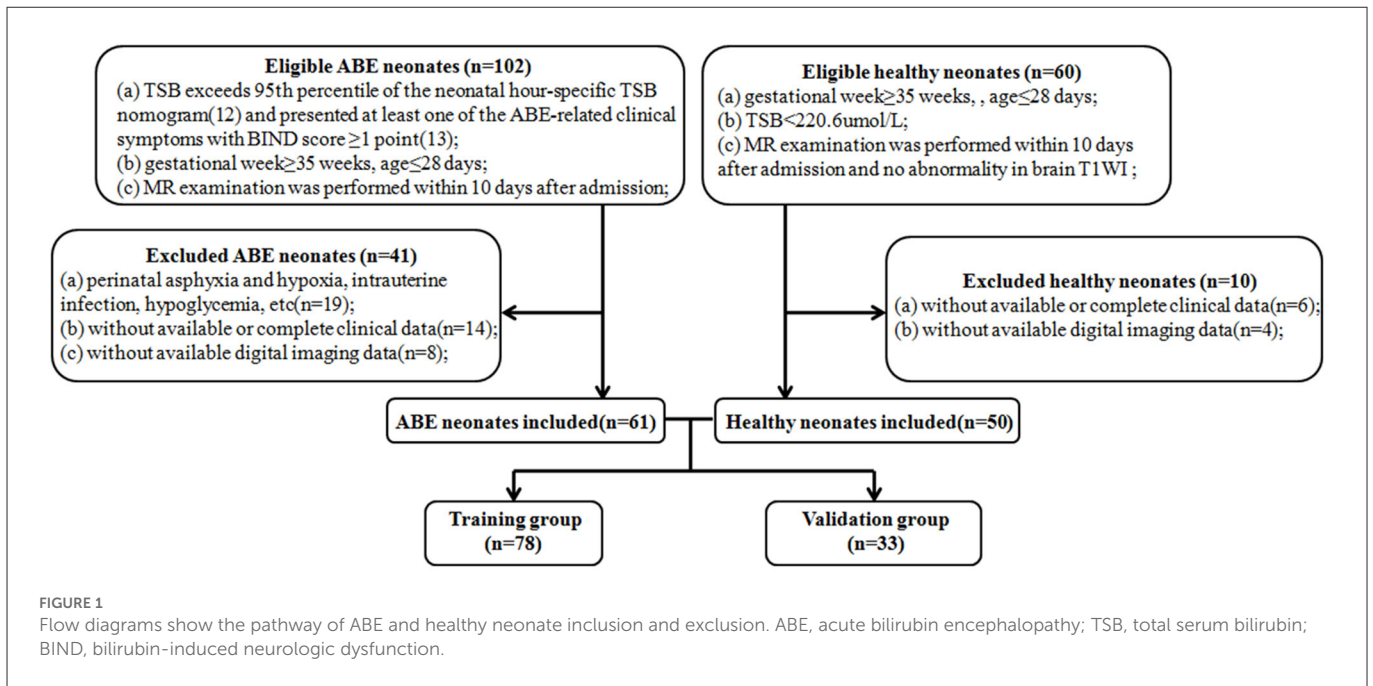
Clinical feature and model

The clinical features in the training and validation group were compared using an independent samples *t*-test (for normally distributed data) or Mann-Whitney *U*-test (for non-normally distributed data) for continuous variables and a chi-squared test for categorical variables.

Features with $P < 0.05$ in the univariate analysis were selected and fed into the multivariate logistic regression analysis using a backward stepwise elimination method based on Akaike's information criterion. The clinical model was established by applying multivariate logistic regression.

Radiomics feature and model

The dimensionality reduction of radiomics features was performed. First, intraclass correlation coefficients were used to assess the intra-observer repeatability of radiomics features. The image segmentation of all cases was performed by observer one with 15 years of experience (JY), and then observer two with 10 years of experience (YL), and used the same method to segment the 30 subjects who were selected from the whole sample based on stratified sampling to reduce possible bias and ensure the reliability of segmentation and feature extraction. Observers



were blinded to clinical and group information. Features with intraclass correlation coefficients > 0.90 were retained, which indicated high robustness and satisfactory reproducibility. Second, maximal relevance and minimal redundancy were performed

to eliminate the redundant and irrelevant features, and 30 features were retained. Then, the least absolute shrinkage and selection operator algorithm was performed to identify the most valuable features. Finally, the radiomics score (rad-score) was

TABLE 1 Patient clinical features between the training and validation groups.

Clinical feature	Training group (n = 78)			Validation group (n = 33)			P-value
	ABE (n = 43)	HC (n = 35)	P-value	ABE (n = 18)	HC (n = 15)	P-value	
Age (d)	8.00 (2.50)	11.00 (11.50)	0.220	9.50 (5.25)	19.00 (4.75)	0.135	0.502
Gender			0.168			0.697	0.315
Male	24 (55.81%)	25 (71.43%)		14 (77.78%)	10 (66.67%)		
Female	19 (44.19%)	10 (28.57%)		4 (22.22%)	5 (33.33%)		
Weight (g)	3224.42 ± 488.03	3447.00 ± 588.04	0.072	3262.22 ± 603.94	3336.00 ± 645.50	0.737	0.885
Gestational week (w)	38.35 ± 1.12	38.56 ± 1.36	0.760	38.42 ± 1.36	38.56 ± 1.51	0.642	0.808
Pregnancy history of maternal			0.820			0.482	0.891
Yes	17 (39.53%)	15 (42.86%)		9 (50.00%)	5 (33.33%)		
No	26 (60.47%)	20 (57.14%)		9 (50.00%)	10 (66.67%)		
Meconium-stained amniotic fluid			0.078			0.375	0.977
Yes	40 (93.02%)	24 (68.57%)		16 (88.89%)	11 (73.33%)		
No	3 (6.98%)	11 (31.43%)		2 (11.11%)	4 (26.67%)		
Premature rupture of membranes			0.649			0.300	0.188
Yes	20 (46.51%)	19 (54.29%)		5 (27.78%)	7 (46.67%)		
No	23 (53.49%)	16 (45.71%)		13 (72.22%)	8 (53.33%)		
Singleton or multiple-birth pregnancy			0.198			1.000	0.366
Singleton	43 (100.00%)	33 (94.29%)		17 (94.44%)	14 (93.33%)		
Multiply	0 (0%)	2 (5.71%)		1 (5.56%)	1 (6.67%)		
Type of delivery			<0.001*			<0.001*	0.342
Spontaneous labor	6 (13.95%)	20 (57.14%)		0 (0%)	8 (53.33%)		
Cesarean delivery	37 (86.05%)	15 (42.86%)		18 (100.00%)	7 (46.67%)		
TSB (umol/L)	387.84 ± 68.17	-		369.39 ± 40.30	-	0.196	
BIND score	3.00 (2.00)	-		3.00 (1.00)	-	0.731	

**p* < 0.05.

calculated based on the selected radiomics features weighted by their coefficients.

Clinical-radiomics model and nomogram

The combined clinical-radiomics model was established to predict the risk of ABE using multivariate logistic regression analysis based on the selected clinical features and radiomics features. To ensure the easy use of the model, the combined clinical-radiomics model was further visualized as a nomogram.

Evaluation

The discrimination performances of the radiologists' visual diagnosis, clinical model, radiomics model, and clinical-radiomics model were assessed by using receiver operating characteristic (ROC) curve analysis. The area under the ROC curve (AUC), accuracy, sensitivity, and specificity were calculated. DeLong's test was used to compare the statistical differences between the AUCs of the training and validation groups. The calibration performance of the combined model was tested by using the calibration curves accompanied by the Hosmer–Lemeshow test; *P* > 0.05 were considered good fitness. The

clinical benefit for clinical application of the combined model was assessed by using decision curve analysis.

The statistical analyses were performed using R software (v. 3.5.3, <http://www.R-project.org>), and two-sided *P* < 0.05 were considered to be statistically significant. The workflow is shown in [Figure 2](#).

Results

Clinical feature and model

Sixty-one neonates with ABE (median age, 9 days; interquartile range, 7–10 days; 35 male) and 50 healthy neonates (median age, 11.5 days; interquartile range, 6–19.75 days; 38 male) were included for the training and validation groups. Demographic and clinical features data are provided in [Table 1](#).

The clinical features were further analyzed by univariate and multivariate logistic regression analysis in the training group ([Table 2](#)). In the univariate analysis, gestational week, meconium-stained amniotic fluid, and type of delivery (*P* < 0.05) were included in the multivariate analysis. Multivariate logistic regression analysis indicated that gestational week and type of delivery (*P* < 0.05) were

TABLE 2 Univariate and multivariate logistic regression analysis of clinical features in the training group.

Clinical features	Univariate analysis		Multivariate analysis	
	Odds ratio	P-value	Odds ratio	P-value
Gestational week	0.45	<0.001*	0.47	0.001*
Type of delivery	8.22	<0.001*	7.53	<0.001*

* $p < 0.05$.

independent risk factors for predicting ABE. The clinical model was established using the above three features.

Radiomics features and model

One hundred features of left GP and 106 features of right GP were considered stable with intra-observer stability (intraclass correlation coefficients ranges: 0.901–1.000 and 0.941–1.000, respectively). These features measured by observer one were selected for subsequent analysis.

There remained ten radiomics features after dimensionality reduction, and the coefficients of these features are presented in [Figure E1](#); these were selected to calculate the corresponding rad-score:

$$\begin{aligned} \text{Rad - score} = & 0.285 + 0.805 \times \text{Right_RunEntropy} + 0.164 \\ & \times \text{Left_Correlation} - 0.049 \times \text{Right_SmallAreaLowGrayEmphasis} \\ & + 0.267 \times \text{Right_SurfaceVolumeRatio} - 0.264 \times \text{Right_Imc1} \\ & - 0.325 \times \text{Left_Maximum2DDiameterRow} - 0.071 \\ & \times \text{Left_Skewness} + 0.12 \times \text{Right_Correlation} + 0.264 \\ & \times \text{Left_GrayLevelNonUniformity_2} + 0.237 \times \text{Left_Idmn} \end{aligned}$$

Clinical-radiomics model and nomogram construction

Combined with the clinical features and the rad-score, the clinical-radiomics model was established. Meanwhile, the nomogram was established based on the clinical-radiomics model to individually estimate the risk of ABE for each neonate ([Figure 3](#)).

Model performance evaluation

The ROC curves and discriminative performance of the clinical model, radiomics model, and clinical-radiomics model are shown in [Figures 4A, B](#) and [Table 3](#). In the training group, the AUC of the clinical model, radiomics model, and clinical-radiomics model was 0.83 ($P < 0.001$, 95% CI: 0.73–0.93), 0.83 ($P < 0.001$, 95% CI: 0.74–0.92), and 0.90 ($P < 0.001$, 95% CI: 0.84–0.97), respectively, with a sensitivity of 0.884, 0.581, and 0.814, specificity of 0.743, 1.000, and 0.914, positive predictive value of 0.809, 1.000, and 0.921, and

negative predictive value of 0.839, 0.660, and 0.800. In the validation group, the AUC of the clinical model, radiomics model, and clinical-radiomics model was 0.86 ($P < 0.001$, 95% CI: 0.72–1.00), 0.79 ($P = 0.005$, 95% CI: 0.63–0.94), and 0.93 ($P < 0.001$, 95% CI: 0.85–1.00), respectively, with a sensitivity of 0.944, 0.778, and 0.944, specificity of 0.800, 0.667, and 0.800, positive predictive value of 0.850, 0.737, and 0.850, and negative predictive value of 0.923, 0.714, and 0.923. DeLong's test showed that there was no significant difference between the training group and the validation group in the clinical model, radiomics model, and clinical-radiomics model ($P = 0.759$, $P = 0.670$, and $P = 0.542$, respectively).

The calibration curve results showed good consistency between the nomogram-predicted probability of ABE and the actual ABE observed in the training group and validation group (Hosmer–Lemeshow test; $P = 0.137$ and 0.362 , respectively) ([Figures 5A, B](#)). The decision curve analysis applied to predict ABE is shown in [Figure 6](#).

Radiologists' visual diagnosis

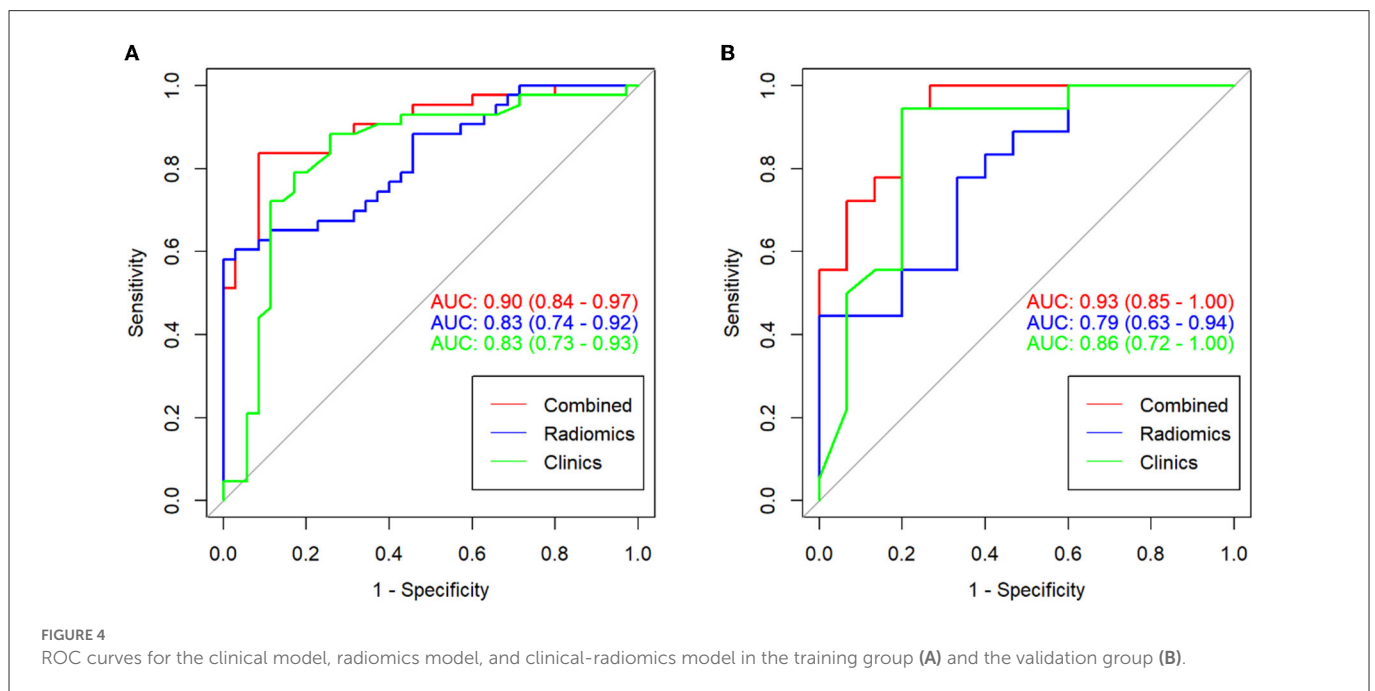
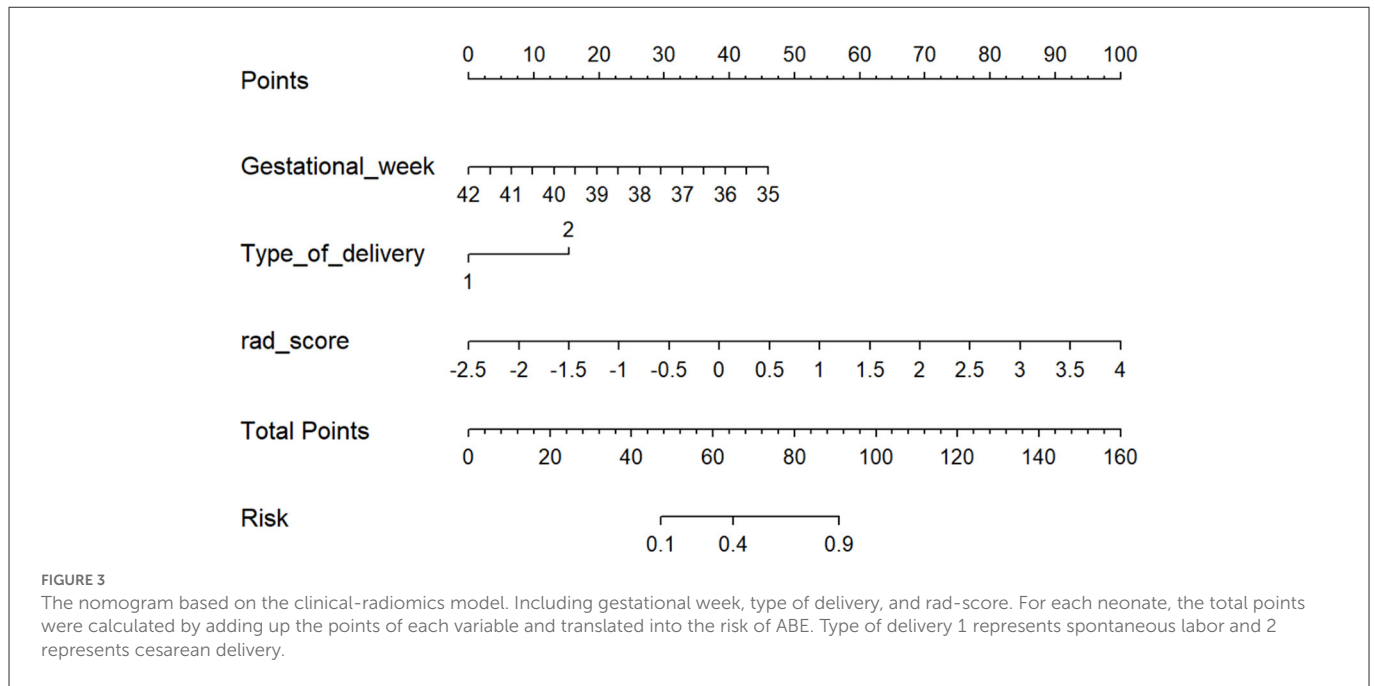
Radiologists' information is shown in [Table E2](#). The AUC of the visual diagnoses of radiologists one and two based on T1WI were 0.57 ($P = 0.215$, 95% CI: 0.46–0.68) and 0.63 ($P = 0.019$, 95% CI: 0.53–0.73), with a sensitivity of 0.377 and 0.459, specificity of 0.760 and 0.800, a positive predictive value of 0.657 and 0.737, and negative predictive value of 0.500 and 0.548, respectively. The AUC of the radiologists' final visual diagnosis was 0.66 ($P = 0.003$, 95% CI: 0.56–0.77), with a sensitivity of 0.508, specificity of 0.820, a positive predictive value of 0.775, and negative predictive value of 0.577. The ROC curves of radiologists' visual diagnosis are shown in [Figure E2](#).

DeLong's test showed that the discriminative performance of the clinical model and clinical-radiomics model in the training and validation groups was increased compared to radiologists' visual diagnosis ([Table 4](#)).

Discussion

Conventional MRI lacks quantitative indicators for brain damage in ABE, and it is impossible to objectively and comprehensively assess the risk of ABE, especially for neonates who may have brain damage when their GPs do not show hyperintensity on T1WI. In this study, we developed and validated a clinical-radiomics model based on T1WI for individualized prediction of ABE, which demonstrated good discrimination, calibration, and clinical benefit. It is worth noting that the discriminative performance of the clinical model and clinical-radiomics model in the training and validation groups was increased compared to that of radiologists with rich experience in pediatric radiology diagnosis. These results indicated that it is difficult to identify the ABE early based on T1WI by the naked eye. Moreover, the sensitivity of radiologists' visual diagnosis was low; however, the models were effectively improved. The nomogram was easy to use and may facilitate personalized risk stratification and further treatment decision-making for neonates with ABE, which could potentially provide a visualized and precise clinical support tool.

ABE is brain damage caused by unconjugated bilirubin passing through the blood-brain barrier (14). The neurotoxicity of unconjugated bilirubin is highly selective, implicating GPs,



the substantia nigra, reticulata, subthalamic nuclei, brain stem, auditory, vestibular, and oculomotor nuclei, the hippocampus, and cerebellum (15); it particularly implicates GPs, which are related to its active metabolism (16). The mechanism of unconjugated bilirubin-induced neuron damage has not been fully elucidated. Existing hypotheses include excitotoxicity hypotheses (17), bilirubin-induced neuroinflammation (18, 19), and oxidative stress mechanisms (20). The destruction of bilirubin on neurons is recoverable in the early stages; consequently, early identification of ABE risk factors and intervention is an important method to prevent ABE, reduce the sequelae, and improve the prognosis.

Gestational week and the type of delivery were considered independent risk factors of ABE and they were incorporated into

the clinical model. For neonates, the earlier the gestational week, especially gestational weeks earlier than 37 weeks, the higher the risk of ABE. This was due to the lower liver enzyme activity in premature infants, which affected the combination of human serum albumin and bilirubin, and premature infants were often treated with antibiotics, which destroyed the intestinal microecological environment. These factors caused bilirubin accumulation and led to ABE (21). The type of delivery also affected the risk of ABE; cesarean births were more likely to develop ABE, and this may be related to anesthesia (22, 23). In the radiomics model, the selected features were composed of the following categories: one first-order feature (Left_Skewness), two shape features (Right_SurfaceVolumeRatio and Left_Maximum2DDiameterRow), and seven texture features (Right_

TABLE 3 ROC curves of models in the training and validation group.

Model	Clinical model	Radiomics model	Clinical-radiomics model
Training group			
AUC (95% CI)	0.83 (0.73–0.93)	0.83 (0.74–0.92)	0.90 (0.84–0.97)
Sensitivity	0.884	0.581	0.814
Specificity	0.743	1.000	0.914
Positive predictive value	0.809	1.000	0.921
Negative predictive value	0.839	0.660	0.800
Validation group			
AUC (95% CI)	0.86 (0.72–1.00)	0.79 (0.63–0.94)	0.93 (0.85–1.00)
Sensitivity	0.944	0.778	0.944
Specificity	0.800	0.667	0.800
Positive predictive value	0.850	0.737	0.850
Negative predictive value	0.923	0.714	0.923
P-value	0.759	0.670	0.542

ROC, receiver operating characteristic; AUC, area under the curve; CI, confidence interval.

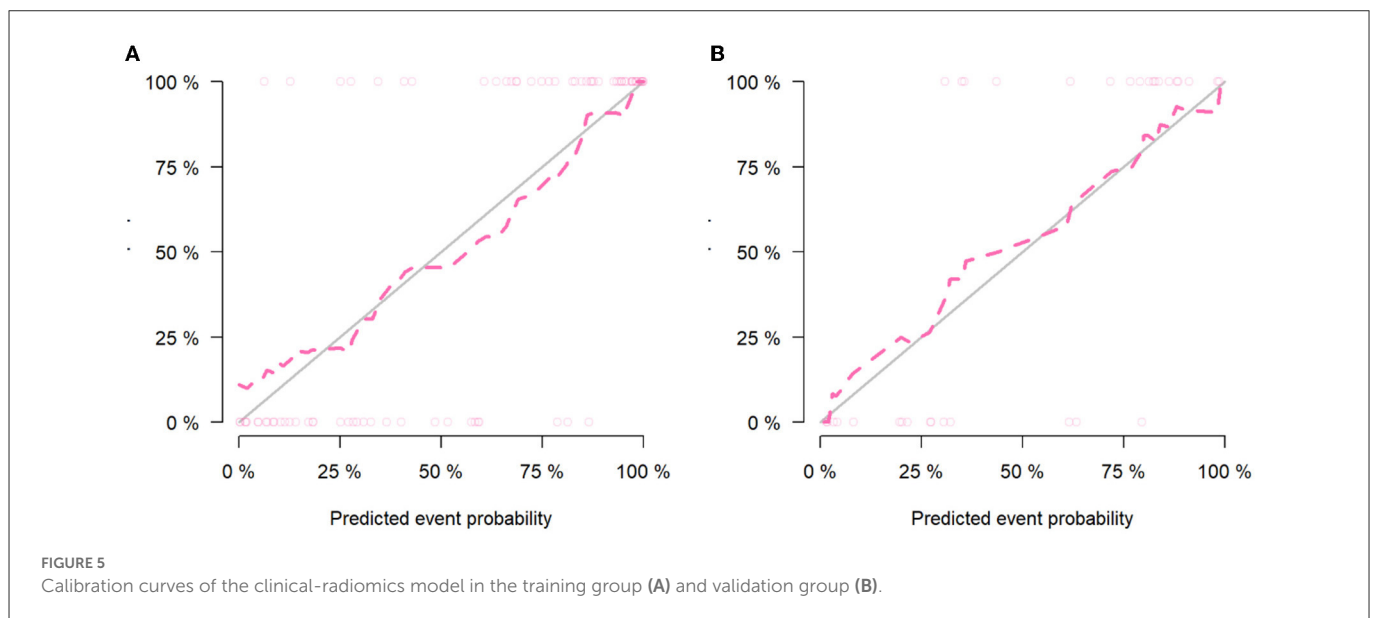


FIGURE 5 Calibration curves of the clinical-radiomics model in the training group (A) and validation group (B).

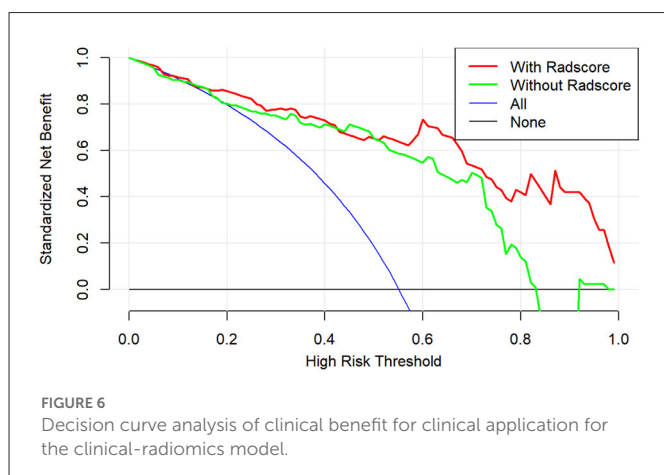


FIGURE 6 Decision curve analysis of clinical benefit for clinical application for the clinical-radiomics model.

RunEntropy, Left_Correlation, Right_SmallAreaLowGrayEmphasis, Right_Imc1, Right_Correlation, Left_GrayLevelNonUniformity_2,

and Left_Idmn). Smaller skewness reflected the left deviation of the image, and more voxels were high intensity. Macroscopically, the higher intensity of left globus pallidus increased the risk of ABE. Smaller Left_Maximum2DDiameterRow and larger Right_SurfaceVolumeRatio were correlated closely with the risk of ABE. We speculated this was due to the neurotoxicity of unconjugated bilirubin increasing the influx of calcium ions, stimulating the activity of proteolytic enzymes, and leading to apoptosis (20, 24), changing the shape and volume of GP. The texture features described the distribution of voxel intensity and the spatial relationship between local adjacent voxels, which were a comprehensive reflection of the intrinsic properties of the image, and they could quantify the complexity of the texture of bilateral GPs in neonatal with ABE. However, associating a single texture feature with complex biological processes remains a challenge. These texture features included in the radiomics model may reflect the heterogeneity of bilateral GPs in neonatal with ABE. Liu et al. (25) also established models to distinguish between ABE and healthy neonates based on T1WI, and the best model obtained good diagnostic efficiency with an AUC of 0.946. Wu et al. (26) integrated

TABLE 4 Comparison of discriminative performance between radiologists' visual diagnosis and models.

Radiologist	Group	Model	P-value
Radiologist 1	Training group	Clinical model	<0.001*
		Rad_score	<0.001*
		Clinical-radiomics model	<0.001*
	Validation group	Clinical model	0.001*
		Rad_score	0.018*
		Clinical-radiomics model	<0.001*
Radiologist 2	Training group	Clinical model	0.003*
		Rad_score	0.002*
		Clinical-radiomics model	<0.001*
	Validation group	Clinical model	0.009*
		Rad_score	0.083
		Clinical-radiomics model	<0.001*
Radiologists' final visual diagnosis	Training group	Clinical model	0.013*
		Rad_score	0.009*
		Clinical-radiomics model	<0.001*
	Validation group	Clinical model	0.023*
		Rad_score	0.171
		Clinical-radiomics model	<0.001*

* $p < 0.05$.

multimodal MRI with deep-learning approaches to diagnose ABE, with the combination of three modalities, T1WI, T2WI, and diffusion-weighted imaging, with an AUC of 0.991 ± 0.007 . However, these studies did not consider clinical factors. The most important thing is that they did not set up independent validation sets to verify the established models. Our study combined clinical and radiomics models and achieved a good prediction performance; the independent validation group verified the established model, and the risk of overfitting was effectively avoided.

Our study had several limitations. First, this was a retrospective study and potential bias may have been introduced in the selection of research subjects; some clinical data such as albumin and blood type were not considered. Furthermore, this batch of data was scanned using the same equipment, the sample size was small, there was a long inclusion period, and a lack of external validation; therefore, a larger cohort of prospective studies based on multicenter data is needed to verify the performance of the clinical-radiomics model. Lastly, the regions of interest in this study were manually placed, which may inevitably lead to certain errors. We have started to develop an automatic segmentation tool for GPs, which can segment the GPs more accurately and robustly in the future.

Conclusions

In conclusion, we developed and validated a combined clinical-radiomics model based on T1WI to predict ABE. The application

of the nomogram could potentially provide a visualized and precise clinical support tool.

Data availability statement

The raw data supporting the conclusions of this article will be made available by the authors, without undue reservation.

Ethics statement

The studies involving human participants were reviewed and approved by the First Affiliated Hospital of Dalian Medical University Ethics Committee. Written informed consent to participate in this study was provided by the participants' legal guardian/next of kin.

Author contributions

JY: conceptualization, investigation, and data curation. YL: data curation and writing – original draft. YJ: validation and visualization. BG: data curation. JW: resources and supervision. YG: software and methodology. LX: methodology. YM: conceptualization, funding acquisition, and writing – review and editing. All authors contributed to the article and approved the submitted version.

Funding

This work was supported by the National Natural Science Foundation of China (grant number 81671646).

Conflict of interest

YG and LX were employed by the GE Healthcare.

The remaining authors declare that the research was conducted in the absence of any commercial or financial relationships that could be construed as a potential conflict of interest.

Publisher's note

All claims expressed in this article are solely those of the authors and do not necessarily represent those of their affiliated organizations, or those of the publisher, the editors and the reviewers. Any product that may be evaluated in this article, or claim that may be made by its manufacturer, is not guaranteed or endorsed by the publisher.

Supplementary material

The Supplementary Material for this article can be found online at: <https://www.frontiersin.org/articles/10.3389/fneur.2023.956975/full#supplementary-material>

References

1. Olusanya BO, Kaplan M, Hansen TWR. Neonatal hyperbilirubinaemia: a global perspective. *Lancet Child Adolesc.* (2018) 2:610–20. doi: 10.1016/S2352-4642(18)30139-1
2. Olusanya BO, Teeple S, Kassebaum NJ. The contribution of neonatal jaundice to global child mortality: findings from the GBD 2016 study. *Pediatrics.* (2018) 141:e20171471. doi: 10.1542/peds.2017-1471
3. GBD 2016 Causes of Death Collaborators. Global, regional, and national age-sex specific mortality for 264 causes of death, 1980-2016: a systematic analysis for the global burden of disease study 2016. *Lancet.* (2017) 390:1151–210. doi: 10.1016/S0140-6736(17)32152-9
4. Tan N, Hu S, Hu Z. Quantitative proteomic characterization of microvesicles/exosomes from the cerebrospinal fluid of patients with acute bilirubin encephalopathy. *Mol Med Rep.* (2020) 22:1257–68. doi: 10.3892/mmr.2020.11194
5. Bahr TM, Christensen RD, Agarwal AM, George TI, Bhutani VK. The neonatal acute bilirubin encephalopathy registry (NABER): background, aims, and protocol. *Neonatology.* (2019) 115:242–6. doi: 10.1159/000495518
6. Bech LF, Donneborg ML, Lund AM, Ebbesen F. Extreme neonatal hyperbilirubinemia, acute bilirubin encephalopathy, and kernicterus spectrum disorder in children with galactosemia. *Pediatr Res.* (2018) 84:228–32. doi: 10.1038/s41390-018-0066-0
7. Govaert P, Lequin M, Swarte R, Robben S, De Coo R, Weisglas-Kuperus N, et al. Changes in globus pallidus with (pre)term kernicterus. *Pediatrics.* (2003) 112:1256–63. doi: 10.1542/peds.112.6.1256
8. Campistol J, Galvez H, Cazorla AG, Málaga I, Iriondo M, Cusi V, et al. Neurological dysfunction induced by bilirubin. *Neurologia.* (2012) 27:202–11. doi: 10.1016/j.nrleng.2010.03.001
9. Wisnowski JL, Panigrahy A, Painter MJ, Watchko JF. Magnetic resonance imaging of bilirubin encephalopathy: current limitations and future promise. *Semin Perinatol.* (2014) 38:422–8. doi: 10.1053/j.semperi.2014.08.005
10. Rogers W, Thulasi Seetha S, Refaie TA, Lieverse RI, Granzier RW, Ibrahim A, et al. Radiomics: from qualitative to quantitative imaging. *Br J Radiol.* (2020) 93:20190948. doi: 10.1259/bjr.20190948
11. Aerts HJ, Velazquez ER, Leijenaar RT, Parmar C, Grossmann P, Carvalho S, et al. Decoding tumour phenotype by noninvasive imaging using a quantitative radiomics approach. *Nat Commun.* (2014) 5:4006. doi: 10.1038/ncomms5644
12. Bhutani VK, Johnson L, Siviert EM. Predictive ability of a predischarge hour-specific serum bilirubin for subsequent significant hyperbilirubinemia in healthy term and near-term newborns. *Pediatrics.* (1999) 103:6–14. doi: 10.1542/peds.103.1.6
13. Johnson L, Brown A, Bhutani V. BIND: A clinical score for bilirubin induced neurologic dysfunction in newborns. *Pediatrics.* (1999) 104:746–7.
14. Silva RF, Rodrigues CM, Brites D. Rat cultured neuronal and glial cells respond differently to toxicity of unconjugated bilirubin. *Pediatr Res.* (2002) 51:535–41. doi: 10.1203/00006450-200204000-00022
15. Cayabyab R, Ramanathan R. High unbound bilirubin for age: a neurotoxin with major effects on the developing brain. *Pediatr Res.* (2019) 85:183–90. doi: 10.1038/s41390-018-0224-4
16. Neknek GA, Woldemichael K, Moges A, Solomon DZ. MRI of bilirubin encephalopathy (kernicterus): a case series of 4 patients from Sub-Saharan Africa, May 2017. *Radiol Case Rep.* (2018) 13:676–9. doi: 10.1016/j.radcr.2018.03.018
17. Usman F, Diala UM, Shapiro S, LePichon JB, Slusher TM. Acute bilirubin encephalopathy and its progression to kernicterus: current perspectives. *Res Rep Neonatol.* (2018) 8:33–44. doi: 10.2147/RRN.S125758
18. Watchko JF, Maisels MJ. The enigma of low bilirubin kernicterus in premature infants: why does it still occur, and is it preventable? *Semin Perinatol.* (2014) 38:397–406. doi: 10.1053/j.semperi.2014.08.002
19. Deliktaş M, Ergin H, Demiray A, Akça H, Özdemir ÖM, Özdemir MB. Caffeine prevents bilirubin-induced cytotoxicity in cultured newborn rat astrocytes. *J Matern Fetal Neonatal Med.* (2019) 32:1813–9. doi: 10.1080/14767058.2017.1419175
20. Watchko JF. Kernicterus and the molecular mechanisms of bilirubin-induced CNS injury in newborns. *Neuromolecular Med.* (2006) 8:513–29. doi: 10.1385/NMM:8:4:513
21. Tufail A, Ahmad I, Arshad R, Yousaf S, Butt MA. Comparison of light-emitting diodelights vs fluorescent light phototherapy for the treatment of unconjugated hyperbilirubinemia in preterm infants-randomised control trial. *J Park Med Assoc.* (2019) 69:767–71.
22. El-Kabbany ZA, Toaima NN, Toaima TN, El-Din MY. Does anaesthesia in mothers during delivery affect bilirubin levels in their neonates? *Korean J Pediatr.* (2017) 60:385–9. doi: 10.3345/kjp.2017.60.12.385
23. Ozcakir HT, Lacin S, Baytur YB, Lülecı N, Inceboz US. Different anesthesiologic strategies have no effect on neonatal jaundice. *Arch Gynecol Obstet.* (2004) 270:179–81. doi: 10.1007/s00404-003-0580-z
24. Falcão AS, Silva RF, Fernandes A, Brito MA, Brites D. Influence of hypoxia and ischemia preconditioning on bilirubin damage to astrocytes. *Brain Res.* (2007) 1149:191–9. doi: 10.1016/j.brainres.2007.02.039
25. Liu Z, Ji B, Zhang Y, Cui G, Liu L, Man S, et al. Machine learning assisted MRI characterization for diagnosis of neonatal acute bilirubin encephalopathy. *Front Neurol.* (2019) 10:1018. doi: 10.3389/fneur.2019.01018
26. Wu M, Shen X, Lai C, You Y, Zhao Z, Wu D, et al. Detecting acute bilirubin encephalopathy in neonates based on multimodal MRI with deep learning. *Pediatr Res.* (2021) 91:1168–75. doi: 10.1038/s41390-021-01560-0